

www.acsanm.org Article

CuO Nanoparticles as Copper-Ion Reservoirs for Elesclomol-Mediated Intracellular Oxidative Stress: Implications for Anticancer **Therapies**

Swaroop Chakraborty,* Prabhat Prakash, Juhi Shah, Chaithra Mayya, Sanjay Singh, Raghavan Ranganathan, Virupakshi Soppina, Eugenia Valsami Jones, and Superb K. Misra*



Cite This: ACS Appl. Nano Mater. 2022, 5, 1607-1620



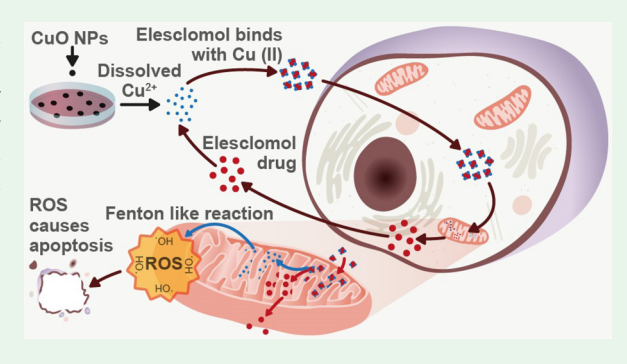
ACCESS I

III Metrics & More

Article Recommendations

Supporting Information

ABSTRACT: Dissolution of metal/metal oxide nanoparticles has been widely exploited to be one of the mechanisms of inducing oxidative stress within bacterial and mammalian cells. Elesclomol has been already evaluated in clinical trials, and the reports have demonstrated a greater therapeutic activity with a prolonged progression-free time for survival of patients. Computational modeling (density functional theory and classical molecular dynamics) and UV-vis spectroscopy analysis showed that the dissolved Cu (II) ions from CuO nanoparticles preferentially bind to Elesclomol in cell culture media. CuO nanoparticles (50-200 ng/mL) when co-delivered with 50 ng/mL Elesclomol drug significantly reduced the cell viability of A549 cells compared to their respective standalone exposure. A time-dependent



study showed a reduced cell viability (up to 80%) and enhanced reactive oxygen species generation (up to three folds), which was explained by the dissolution profile of CuO nanoparticles. Stable isotope tracing confirmed the intracellular accumulation of copper inside A549 cells to increase by up to four times when 1000 ng/mL ⁶⁵CuO nanoparticles were exposed in the presence of 50 ng/mL Elesclomol. The cytotoxicity was rapid, with 70% of the cell death occurring within the span of 12 h through apoptosis pathways with a very minimal drug concentration. In our work, we exploited the ability of CuO nanoparticles to act as a reservoir with slow and sustained release of Cu (II) ions to bind with Elesclomol, which helped in enhanced generation of intracellular oxidative stress and can be used as a promising approach for Elesclomol-based anticancer therapy.

KEYWORDS: dissolution, oxidative stress, Elesclomol, nanoparticles, tracing, molecular dynamics, DFT

1. INTRODUCTION

Cancer is known to be one of the primary causes of death and has become one of the major health concerns worldwide. Currently, there are several treatment options available for cancer such as surgery, chemotherapy, radiotherapy, and so on, yet the use of such an intervention in general becomes unaffordable and causes side effects that leads to reduction in the use of cancer treatment options. Due to these limitations, there is a requirement of effective, inexpensive, and biocompatible intervention that can be affordable and of high efficacy in the treatment. One such approach is reactive oxygen species (ROS)-mediated oxidative therapy.

Metal oxide nanoparticles such as CuO, ZnO, and so on have been reported to induce cell death via inducing oxidative stress inside the cells. These metal oxide nanoparticles induce cancer cell death through the mechanism such as "Trojan Horse" and "Fenton reaction." The oxidative stress is facilitated by an enhanced release of metal ions in biological milieu and interfering with the electron transport chain within mitochondria to generate dissolved ionic species.² The

alternation of ATP production pathways results in the enhanced production of ROS inside mitochondria. Cancer cells adapt to such high ROS production and get resistant to the majority of chemotherapeutic drugs. However, uncontrolled ROS production beyond threshold in a cancer cell can be a potential target for oxidative therapy.³

Elesclomol (1-N',3-N')-bis (benzenecarbonothioyl)-1-N',3-N'-dimethylpropanedihydrazide) triggers the anticancer activities by increasing the production of ROS and subsequently activating the apoptotic pathway. Clinical trials of Elesclomol have demonstrated a greater therapeutic activity with a prolonged progression-free time for the survival of the patient.⁴ The functioning of the Elesclomol drug is elicited by its high

Received: December 15, 2021 Accepted: December 19, 2021 Published: January 4, 2022





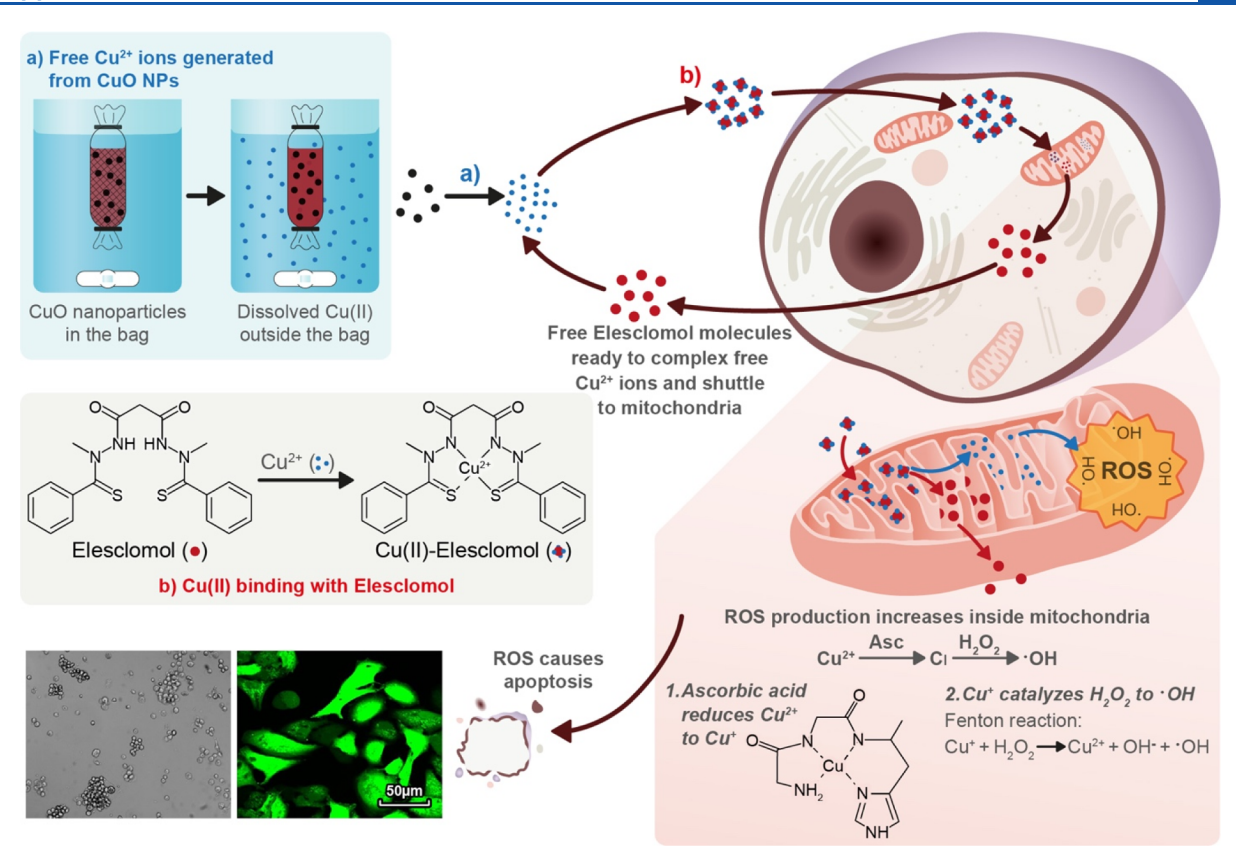


Figure 1. Schematic showing dissolved Cu(II) binding to free Elesclomol and forming the Cu(II)-Elesclomol complex and the mechanism of ROS generation once Elesclomol delivers Cu(II) ions inside mitochondria.

binding affinity to Cu (II) ions and selectively transports Cu (II) ions to mitochondria and creates an alteration in the electron transport chain.⁵ Elesclomol binds with Cu (II) ions and forms a neutral complex. According to the X-ray structure reported by Yadav et al. (2013), the bivalent Cu binds to Elesclomol through the loss of two protons from the N1 and N2 atoms of Elesclomol molecules and forms a neutral complex. The Elesclomol drug has a significantly high affinity toward copper (II) ions with a binding affinity value of $10^{24} \times$ 1 M⁻¹. The bonding of Cu (II) is very strong with Elescomol, and it is expected to have a slow dissociation of Cu (II) from the complex. Research results have reported that Cu-Elesclomol complexes are 1040 folds and 34 folds more potent than Pt-Elesclomol complex and Ni-Elesclomol complex, respectively, in reducing the cell viability of K562 cells. As shown in Figure 1, the free Elescomol drug makes a stable complex with Cu (II) ions by donating four lone pairs and that makes the complex more hydrophobic in nature. Such enhancement in hydrophobicity increases the uptake of the Cu-Elesclomol complex by the cells; hence, more amount of Cu (II) enters the mitochondria to enhance the ROS production.⁵ Nagai et al.⁵ demonstrated the efficacy of the Elesclomol drug to chelate free Cu (II) ions and selectively transfer Cu ions to mitochondria and induce oxidative stress in cancer cells. The dissociation of Cu (II) ions from Elesclomol occurs because of a highly reducing environment of mitochondria. As shown in Figure 1, the reducing groups like ascorbic acid plays a major role in reducing Cu (II) to Cu (I). Since Elesclomol can only form complexes with Cu (II), the reduced Cu (I) immediately disassociates with the complex and that makes Elesclomol available freely to complex with the

other available free Cu (II) ions. The previously reported work mainly discussed the delivery of the Cu (II)—Elesclomol complex to the cells at a certain concentration to induce oxidative stress. It was identified that the bioavailability of Cu (II) ions acts as a limiting factor because once the Elesclomol delivers the Cu (II) ions inside the cells, the drug molecules efflux out from the cells to form complexes with other available free Cu ions. However, the free Cu ions are not readily available in the extracellular matrix because they form organic/inorganic complexes.

In addition to experimental methods, computer simulations are widely used as a tool to model drug-metal ion binding and spectral elucidation.^{7,8} While molecular dynamics (MD)-based simulations are performed to understand atomic scale interactions in the condensed phase of the drug-ion binding, a detailed and more accurate information about the energetics and spectra can be extracted from quantum mechanics-based density functional theory (DFT) calculations. 9,10 In case of the metal ion-drug environment, competitive interactions of the metal ion with the drug versus the constituents of medium affect the binding affinity. Since dissolution media like Dulbecco's modified Eagle's medium (DMEM) contains various amino acids, their cooperative effects on drug-ion binding dictate the extent of binding. The relative affinity of metal ion for amino acids versus drug or among amino acids can be modeled using DFT calculations. In our study, we are using CuO nanoparticles as the reservoir to maintain a sustained release of Cu (II) ions until the nanoparticles are completely dissolved in the biological media. The slow and sustained release of Cu (II) ions will provide a time lag to Elesclomol molecules to capture other free Cu (II) ions and

deliver it inside mitochondria. The process helps reducing the dosage requirement of Elesclomol and CuO nanoparticles because of their synergistic effect in inducing oxidative stress and can be a promising approach toward enhanced oxidative stress-based anticancer therapy.

2. MATERIALS AND METHODS

2.1. Materials. All the chemicals used were of analytical grade. CuCl₂·2H₂O, NaOH, and acetic acid were procured from Himedia Ltd, India. ⁶⁵CuCl₂ was obtained from Trace Sciences International, USA. The biological assays, that is, MTT, Annexin V, DCFDA, mitochondrial membrane potential assay kit, and ROS assay kit were obtained from Sigma-Aldrich, USA. The inductively coupled plasmamass spectroscopy (ICP–MS) standards were procured from PerkinElmer Ltd, USA.

2.2. Synthesis and Characterization of CuO and 65CuO Nanoparticles. CuO nanoparticles were synthesized using a coprecipitation reaction in a water reflux system. 12 0.511 g of CuCl₂· 2H₂O was added to 150 mL of deionized water under stirring conditions followed by addition of 500 μ L of glacial acetic acid. The solution was heated to 100 °C, and under vigorous stirring, 0.65 g of NaOH was added and left for 10 min. The black precipitate was washed multiple times with deionized water to obtain a phase pure CuO nanoparticles. Isotopically enriched ⁶⁵CuO nanoparticles were prepared using the abovementioned protocol. The isotopic precursors used to synthesize were 99% enriched and procured from Trace Sciences (USA). The concentration of synthesized CuO nanoparticles was measured using inductively coupled plasma-optical emission spectroscopy (Avio 200, PerkinElmer, USA) and found to be 4619 mg/L. The morphology of CuO nanoparticles was investigated with the help of transmission electron microscopy (TEM, FEI 200 KV). The identification of the compound along with its phase purity was made by X-ray Diffractometer analysis (Bruker D8, Cu K α , 40 kV, 30 mA, $2\theta = 20-80^{\circ}$). Hydrodynamic size and time-dependent suspension stability studies of CuO nanoparticles in DMEM media were performed using dynamic light scattering (Nano ZS, Malvern Instruments, UK) at a concentration of 25 mg/L and at 37 °C (pH =

2.3. CuO Nanoparticle Dissolution-Mediated Elesclomol Binding Studies. Dissolution-mediated Cu (II) binding to Elesclomol experiments were conducted by taking 25 mg/L CuO nanoparticles in a dialysis bag (MWCO: 3.5 kDa, Snakeskin, Thermo Fisher) for 24 h in DMEM (Gibco, Invitrogen). Outside the dialysis bag was 50 mL of phenol red-free DMEM and 10 μ g/mL Elescomol (Enzo Life sciences, USA) at 37 °C. By incubating CuO nanoparticles inside the dialysis membrane and suspending the membrane in phenol red-free DMEM media, we allowed the passage of copper ions through the dialysis membrane. The changes in the spectral pattern of Elesclomol due to its binding with Cu (II) was recorded with time using UV-vis measurements (PerkinElmer UV vis Lambda 365). Similarly, temporal release of dissolved Cu ions from CuO nanoparticles was measured using ICP-MS analysis (Nexion 2000, PerkinElmer, USA). The fate of dissolved Cu (II) ions in biological media was assessed by geochemical modeling using MINTEQ (Visual MINTEQ 3.1).

2.4. DFT and MD Studies. The Cu (II)—Elesclomol interactions and binding are modeled using classical MD simulations (GROMACS 5.0.7 software) and DFT calculations (Gaussian 09 software). To model binding in the condensed phase, aqueous solutions of Elesclomol with amino acids were modeled with Cu (II) ions. 50 Elesclomol molecules (doubly deprotonated), 50 each of six amino acids (Cys, Ser, Thr, Tyr, Asp⁻, and Glu⁻), 50 Cu (II) ions, variable numbers of Na⁺ and Cl⁻ ions, and ~10000 water molecules were used for the initial input construction. In the classical MD framework, OPLS-AA force—field parameters¹³ for bonded and non-bonded interactions were used, except for the atomic partial charges for Coulombic interactions, which were derived from the electrostatic potential using DFT calculations. The details for MD simulations, DFT calculations, and modified set of the atomic partial charges are

provided in the Supporting Information. All classical MD simulations were performed using GROMACS-5.0.7 software package. 17

For the calculation of charge transfer and theoretical UV–vis spectra, calculations were performed with Gaussian 09, Revision E.01 package. ¹⁸ The geometry of Elesclomol and Cu (II)–Elesclomol complexes optimized using PBE functional with LanL2DZ effective core potential was used for Cu (II) ions, and Pople's 6-31+G(d,p) basis was used for other atoms. In case of the Cu (II)–Elesclomol complex, deprotonated geometry was used. The details of DFT and time-dependent-density functional theory (TD-DFT) calculations are provided in the Supporting Information.

2.5. Cell Viability. MTT assay was performed to evaluate the mitochondrial activity of A549 cells. ²¹ 96-well plates were seeded with 5×10^3 cells/well, and after 24 h of incubation, the cells were treated with (a) Elesclomol (1–1000 ng/mL), (b) Cu ions (1–20000 ng/mL), (c) Cu ions (1–1000 ng/mL) and Elesclomol (50–500 ng/mL), (d) CuO nanoparticles (10–20,000 ng/mL), and (e) CuO nanoparticles (10–500 ng/mL) and Elesclomol (50 ng/mL). CuCl₂· 2H₂O was used as the source of Cu (II) ions. 2% H₂O₂ was used as a positive control, and phosphate buffer saline (PBS) was used as a negative control. Total and time-dependent cell viability was quantified by measuring the absorbance of the dissolved formazan product at 590 nm (Biotek, Synergy HT spectrophotometer), and simultaneously cell morphology was assessed using a phase-contrast microscope for a period of 24 h. The formula used for calculating the cell viability was

$$\frac{\text{Abs}_{590} \text{ sample-Abs}_{590} \text{ medium}}{\text{Abs}_{590} \text{ control-Abs}_{590} \text{ medium}} \times 100$$
(1)

2.6. ROS Assay. In a time-dependent experiment, the cells (seeding density of 1.2×10^5 cells) were exposed to two concentrations of drugs (10 and 50 ng/mL), along with three concentrations of CuO nanoparticles and Cu ions (50, 100, and 200 ng/mL). Post-treatment, the fluorescence intensity was measured using a multimode plate reader spectrophotometer (Biotek, Synergy HT spectrophotometer). For intracellular ROS imaging, 5.0×10^4 cells were grown on pretreated glass coverslips for 24 h at 37 °C and exposed to 50 ng/mL Elesclomol, CuO nanoparticles (100 and 200 ng/mL), and a combination of both for 3 h. The cells were rinsed with 1× PBS, treated with 300 μ L of DCFDA dye (concentration = 20 μ M), and incubated for 30 min at 37 °C. The cells were washed with 1× PBS, and the cover slips were mounted on a clean glass slide with the prolong gold antifade mounting agent (Thermofisher Scientific) with DAPI and imaged using a confocal microscope (Leica) and phase-contrast microscope (Nikon).

2.7. Annexin V Apoptosis Assay. Apoptotic/necrotic cell population can be recognized by staining cells with fluorescein isothiocyanate conjugated (FITC)-Annexin V and propidium iodide (PI) dye as per the manufacturer's protocol (BioVision, Milipitas, CA, USA). Briefly, 12-well plates were used to seed 1.5×105 cells and incubated for 24 h. Cells were then treated with various combinations of Eleschomol and CuO nanoparticles for 6 and 10 h. Afterward, cells were harvested and washed with PBS, re-suspended in 0.4 mL of binding buffer containing 5 μ L of FITC-Annexin and 5 μ L of PI, and incubated for 10 min in the dark at room temperature. Cells were analyzed using a flow cytometer (BD FACS Calibur, BD Biosciences, CA).

2.8. Mitochondrial Membrane Potential Assay. The effect of CuO nanoparticles with and without Elesclomol on the mitochondrial membrane potential (MMP; $\Delta \psi$) of A549 cells was assessed utilizing cationic dye JC-1 as per the manufacturer's protocol (Cayman Chemicals, Ann Arbor, Michigan, USA). Briefly, black clear bottom 96-well plates were used to seed 1×10^4 cells and were incubated until it reaches 80% confluency at 37 °C, 5% CO₂. After the incubation, the cells were treated with various combinations of Elesclomol and CuO nanoparticles for 3 and 6 h. Cells were incubated with 10 μ L of JC-1 dye (dye was diluted in the 1:10 ratio in culture medium) for 20 min at 37 °C in the dark, 5% CO₂. The plate was centrifuged for 5 min at 400 × g, and the supernatant was discarded.

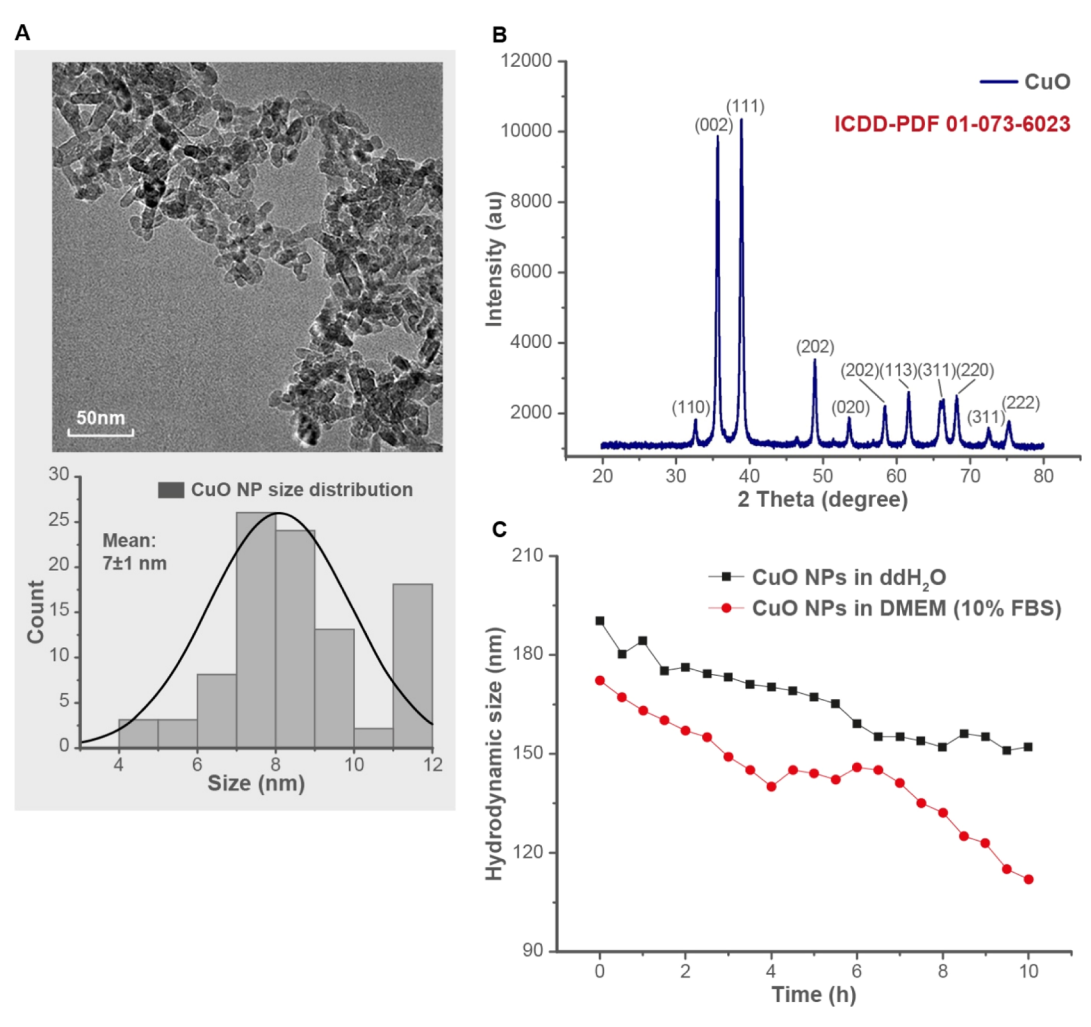


Figure 2. Characterization and stability studies of CuO nanoparticles. (A) TEM image and size distribution of CuO nanoparticles (number of particles = 100), (B) X-ray diffractogram of CuO nanoparticles, and (C) suspension stability of CuO nanoparticles in DMEM media and in deionized water.

Cells were washed twice with assay buffer. Afterward, 100 μ L of assay buffer was added to each well. The mitochondrial membrane potential was represented as the ratio of red:green fluorescence and estimated using a multiwell plate reader (BioTek Synergy HT).

2.9. Live Cell Imaging. Live cell imaging was performed to investigate the time-dependent ROS generation and changes in the cellular behavior on exposure to standalone Elesclomol (50 ng/mL), CuO nanoparticles (200 ng/mL), and the codelivery of both as compared to the control. 20×10^3 cells were seeded in the glass bottom plates (Nunc, Thermo fisher Scientific) and incubated for 24 h in 37 °C, 5% CO₂. After incubation, the cells were stained with Hoechst and 10 μ M DCFDA dye in serum-free DMEM and were incubated for 30 min. After incubation, the cells were washed with 1× PBS and were exposed to various combination of Elesclomol and CuO nanoparticles and transferred to live cell imaging setup in confocal microscopy (Leica). Time-dependent images were captured for 12 h to observe the ROS generation and changes in the cell morphology.

2.10. Intracellular Trafficking of Cu. To test the efficacy of the Elesclomol drug in transporting Cu (II) ions into the cells, intracellular 65 Cu concentration was measured. In this experiment, 1000 ng/mL 65 Cu ions (65 CuCl $_2$ was used as the source of Cu (II) ions) and equivalent 65 CuO were exposed to the cells (8.0 × 10 5 cells) with and without Elesclomol (50 ng/mL). After incubating for 4 h, the cells were washed with 1× PBS and treated with trypsin for harvesting the cells. The harvested cells were pelletized, freeze-dried, and digested using a wet ashing procedure. The ratio of HNO $_3$ /H $_2$ O $_2$

was 3:1, wherein 4.5 mL of HNO_3 was mixed with 1.5 mL of H_2O_2 to digest the sample under heating conditions. The calibration curve in the concentration range of 0.00001–1 μ g/mL using ⁶⁵Cu ionic standard (99%, 10 μ g/mL, Inorganic ventures, USA) was prepared and measured using ICP–MS (Nexion 2000, PerkinElmer, USA). The measurements were carried out in the Helium KED mode.²²

2.11. Statistical Analysis. Biological experiments were carried out in triplicate (n=3), and the data are presented as mean \pm standard deviation. Student's t test was performed to obtain the p-value of the independent experimental variable (CuO, Cu ions, and Eleschomol groups) compared to the control. The differences were statistically significant at values of p < 0.05, p < 0.01, and p < 0.001.

3. RESULTS AND DISCUSSION

3.1. Characterization of CuO Nanoparticles. TEM micrographs of CuO nanoparticles are shown in Figure 2A, and the average size for CuO nanoparticles was 7 ± 1.15 nm. XRD analysis demonstrates CuO nanoparticles to be phase pure with an average crystallite size of 6.49 nm and having a monoclinic lattice structure (ICDD-PDF 01-073-6023) (Figure 2B). The miller indices (hkl) of the respective XRD peaks are shown in Figure 2B. 65 CuO nanoparticles synthesized in this study were used only for quantifying intracellular accumulation of Cu upon treatment with Elesclomol. For the rest of the studies, non-isotopically enriched CuO nano-

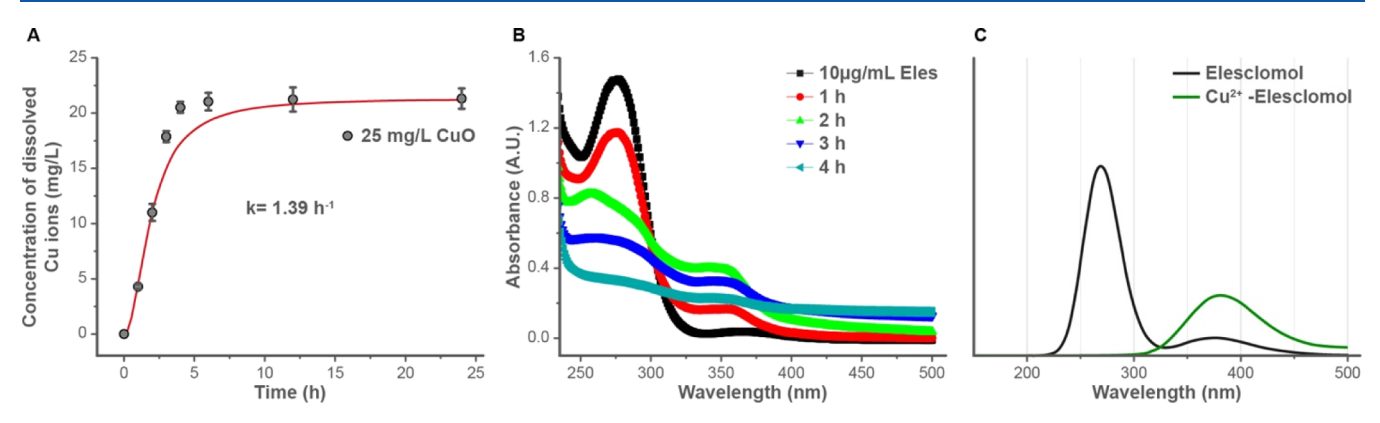


Figure 3. (A) Dissolution profile of CuO nanoparticles in DMEM media. (B) CuO dissolution-mediated Elesclomol-copper ion complex formation at different time points. (C) Theoretical UV-vis spectra from DFT calculations showing a $\lambda_{\rm max}$ of 275 nm for Elesclomol and $\lambda_{\rm max}$ of 380 nm for the Cu(II)-Elesclomol complex.

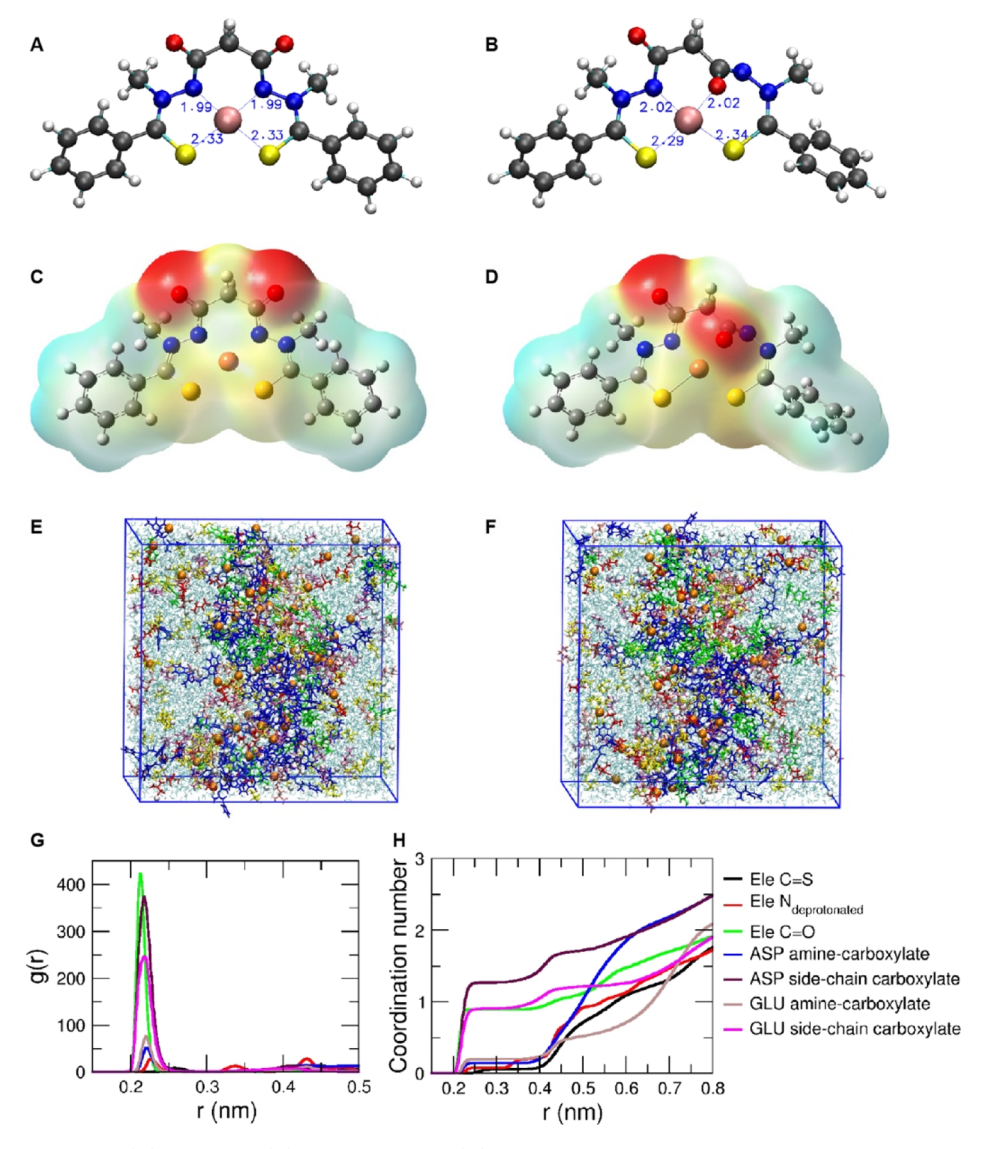


Figure 4. Optimized geometries (A) GM1 and (B) GM2 of the Cu (II)—Elesclomol complex obtained from PBE/LanL2DZ&6-31+G(d,p) DFT calculations; (C) GM1 and (D) GM2 show the electrostatic potential mapped on the electron density obtained from DFT calculations. Snapshots from classical MD simulation under NVT ensemble conditions at (E) t = 20 ns, (F) t = 30 ns.: orange (balls)—Cu(II), white (balls)—Na⁺, cyan, transparent (sticks)—water, blue (sticks)—Elesclomol (red, pink, magenta, yellow, and green) (sticks)—amino acids. (G) Radial distribution and (H) coordination number of various Elesclomol and amino acid-binding sites around Cu (II) from t = 10 ns to t = 30 ns from the production run under NVT conditions.

particles were used. Characterization of ⁶⁵CuO nanoparticles is shown in Supporting Information (Figure S1, size: 8.5 ± 1.65 nm). Suspension stability of CuO nanoparticles was measured by conducting a time-dependent hydrodynamic size measurement of CuO nanoparticles in DMEM and deionized water. Analysis showed that the average hydrodynamic size of CuO nanoparticles in deionized water at time t = 0.5 h was 180 nm and reduced to 152 nm after 10 h (Figure 2C). The reduction of hydrodynamic size of CuO nanoparticles is because of sedimentation of bigger particles in deionized water. 12,23,24 In the case of DMEM [10% fetal bovine serum (FBS)], at time t= 10 h, the average hydrodynamic size was reduced to 112 nm. Possible reasons for the size reduction are interactions of CuO nanoparticles with ionic species dispersed in DMEM media leading to dissolution. 12 The presence of amino acid, such as folic acid acting as a weak oxidizing agent in the media, facilitates enhanced dissolution of CuO nanoparticles.²

3.2. Dissolution of CuO Nanoparticles and Elesclomol-Cu (II) Complexation. Based on the CuO dissolution experiment in DMEM media (Figure 3A), 19.2 ± 1 wt % (4.8) \pm 0.25 mg/L) of CuO nanoparticles dissolved within 1 h of incubation. The modified first-order rate equation was used to perform the best fit of the dissolution profile at different time points and to calculate the rate of dissolution. 11 The dissolution rate (k = 1.39 h⁻¹) was high with almost 82.6 \pm 1 wt % (20.5 \pm 0.50 mg/L) of the nanoparticles dissolving in the first 4 h and saturating to 85.2 ± 3.6 wt % (21.3 ± 0.9 mg/ L) by 24 h of incubation. UV-vis spectroscopy analysis was performed in order to demonstrate Elesclomol binding with copper ions. The Elesclomol suspended in the DMEM was available for complexation with the dissolved and released Cu (II) ions. Figure 3B shows the UV-vis spectrum of the Elesclomol drug as a control (10 μ g/mL), with the maximum absorbance at 279 nm. After 1 h of dissolution of CuO nanoparticles, there was a significant decrease in the peak intensity at 279 nm, indicating the binding of Elesclomol with copper ions (Figure 3B). On increasing the time, there was a gradual change in the main peak of Elesclomol at 279 nm and a concomitant emergence of an absorption peak at 360 nm (due to the spontaneous formation of Cu-Eleschomol complexes). However, there is a significant generation of Cu ions from the CuO nanoparticles, and the Cu (II) ions bind to the Elesclomol molecule at 1:1 M ratio and start to precipitate. It is the reason why the characteristic peak of Elesclomol starts shifting and becomes flattened later when all Elesclomol molecules formed complex with free Cu (II) ions. The formation of the Cu-Elesclomol complex can be observed from its characteristic peak at 365 nm. Although the medium is aqueous and the complex is electrophoretically neutral, the Cu (II)—Elesclomol complex precipitates, and the peak at 365 nm is not observed after 4 h. However, this complex formation and precipitation did not show any impact in the bioavailability of Cu (II)-Elesclomol complex to A549 cells, as demonstrated through ROS assay and cell viability assay. It is because, once the free Elesclomol molecule forms complex with Cu (II) ions, the structure of the Elesclomol molecules changes from distorted to planar (Figure 4A,B), which facilitates active uptake of the Elesclomol–Cu (II) complex inside the cells.⁶ The Elescomol in DMEM (10 μ g/mL) was found to be stable for a period of 4 h (Figure S2). A slight reduction in the peak intensity of Elesclomol can be because of unwanted complexation of Elesclomol with other divalent metal ions present in media.

3.3. Validation of Elesclomol-Cu (II) Binding Using MD and DFT Studies. To investigate the extent of free Cu (II) ions available to bind with Elesclomol, geochemical modeling using MINTEQ software was performed for copper salt in biologically relevant media (viz. simulated body fluid and artificial lysosomal fluid). The modeling data showed that in more complex biological media, the availability of free Cu (II) ions reduced significantly as it readily forms complexes with the various organic/inorganic molecules. For example, in artificial lysosomal fluid, 98% of Cu (II) ions are present in Cu-organic complexes with <1% Cu (II) ions existing in the free state. Similarly, in case of the simulated body fluid, MINTEQ analysis showed that 36% of Cu (II) ions are present in Cu-organic complexes, 54% Cu-inorganic complexes, and remaining 10% as Cu (I) and Cu (II) ions. 12 Therefore, the condensed phase model was simulated using classical OPLS-AA force field¹³ to understand the competitive behavior of Cu (II) ions binding with Elesclomol/amino acids present in the biological fluids. 50 molecules of each amino acid in water (1:100 molecular ratios) were simulated first to prepare and benchmark individual amino acid solutions. 50 molecules of each amino acid along with 50 Elesclomol molecules were equilibrated in a box of the side of 10 nm. 50 Cu (II), Na⁺, and Cl⁻ ions and ~10000 water molecules were used to solvate the mixture thoroughly. After equilibration at T = 350 K under isothermal-isobaric ensemble, the system was cooled to T = 300 K for the final production run (Figure 4E,F). Radial distribution of more negatively charged atoms carboxylate groups of Asp and Glu, and C=S, C=O, N of deprotonated Elesclomol molecules around Cu (II) ions—was calculated (Figure 4G). The computed radial distribution function (RDF) suggests C=O (Elesclomol) to be the most strongly interacting site with Cu (II) ions. While Asp has a slightly higher coordination with Cu (II) ions, the presence of three types of sites (C=O, C=S, N^- , total six on each Elesclomol molecule) suggests Elesclomol to be the preferred host for Cu (II) ions (Figure 4H).

The results from classical simulation also led to the examination of local geometries. In addition to already known tetradentate N⁻, N⁻, S, and S coordinated geometry, GM1, proposed by Wu *et al.*¹⁴ (Figure 4A), another geometry was also discovered during various potential energy scans of Cu (II) with doubly deprotonated Elescomol (Figure 4B). The new geometry (N-, O, S, and S coordinated), GM2, is slightly higher in energy than the other. This geometry could be the initial key configuration which is formed first and later transforms to the more stable configuration (Figure 4A). In addition to the geometrical information, Figure S3 also shows the distribution of atomic partial charges in the local geometries calculated using the CHELPG method. 15 It suggests a net charge transfer from Cu (II) to Elesclomol² to be 1.365 e⁻ for GM1 and 1.240 e⁻ for GM2. The electrostatic potential is mapped on the surface of electron density to exhibit the charge distribution in the geometries (Figure 4C,D). To validate the hypothesis that the decrease in a 279 nm peak and emergence of a 360 nm plateau could be a signature of Cu (II)-Elesclomol binding, TD-DFT calculations were performed using the PBE/LanL2DZ & 6-31+G(d,p) method (details are provided in the Supporting Information) to calculate theoretical UV-vis spectra for Elesclomol and Cu (II)-Elesclomol complex (GM1 geometry). The calculated spectra (Figure 3C) suggests that for Elesclomol, the highest intensity peak appears at 275 nm, and

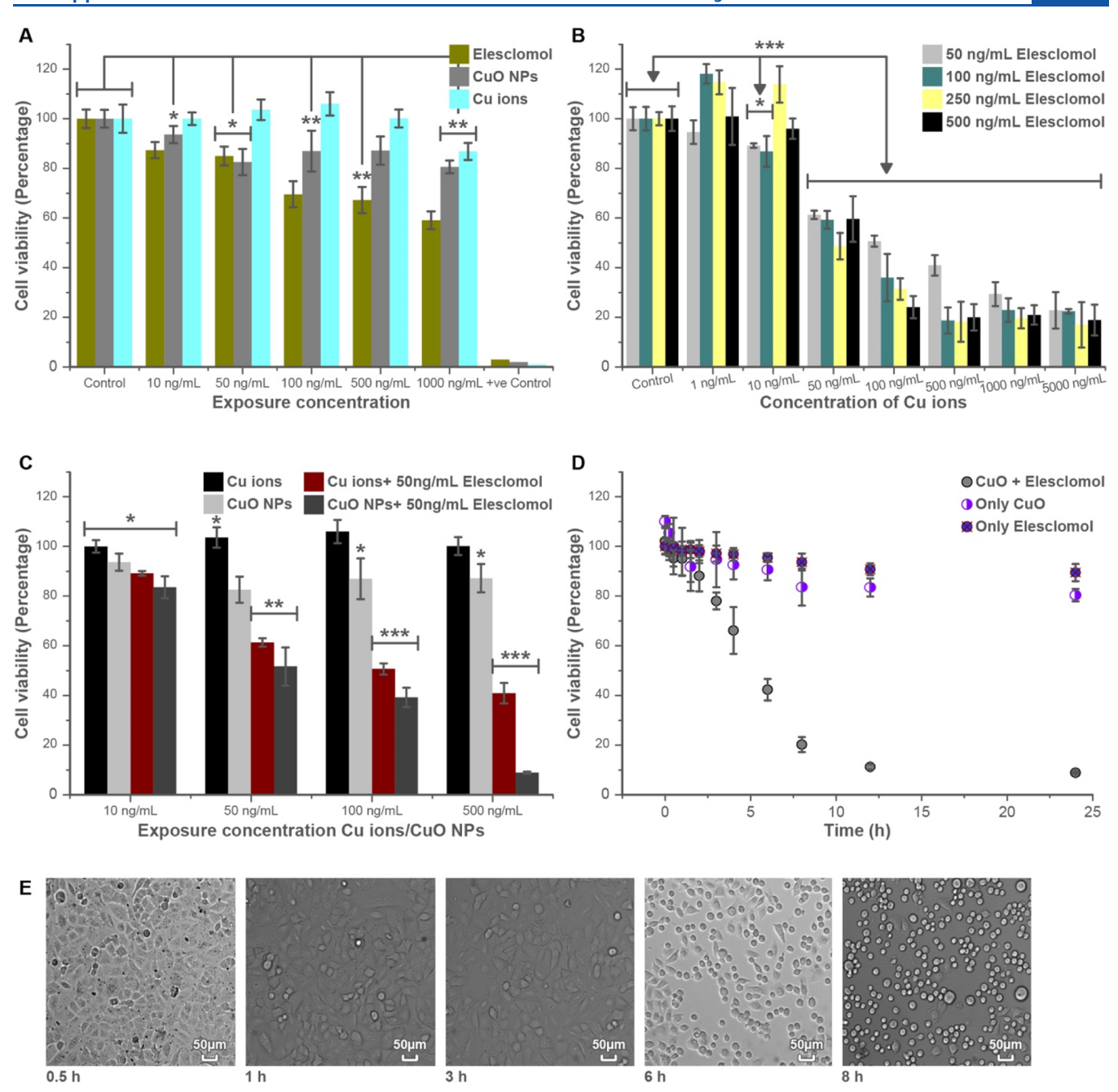


Figure 5. Cytotoxicity study in A549 cells after 24 h of incubation with (A) varying concentrations of Elesclomol, Cu ions, and CuO nanoparticles. (B) Cu ions in a range of concentration with Elesclomol. (C) Cu ions, CuO nanoparticles, Cu ions + Elesclomol, and CuO nanoparticles + Elesclomol. (D) Time-dependent cell viability measurement of A549 cells upon exposure to Elesclomol (50 ng/mL), CuO nanoparticles (500 ng/mL) + Elesclomol (50 ng/mL). (E) Morphology of A549 cells is shown at selected time point after the exposure to CuO nanoparticles (500 ng/mL) + Elesclomol (50 ng/mL). Data represented as mean \pm standard deviation (n = 3). *p < 0.05, **p < 0.01, ***p < 0.001, and ****p < 0.0001. The absorbance was recorded at 590 nm, and the viability of untreated control cells was considered as 100%. Statistical analysis was performed compared to control.

for Cu (II)—Elesclomol complex, the peak appears at 380 nm. Thus, the calculated spectra from TD-DFT not only produce a close agreement with experimental values (Figure 3B) but also validate the hypothesis of the plateau at 360 nm in the experimental spectra to be a peak corresponding to the Cu (II)—Elesclomol complex.

3.4. Co-delivery of CuO Nanoparticles and Elesclomol: Cell Viability. Cell viability of A549 (pulmonary adenocarcinoma) cells was studied after the exposure of (i) Elesclomol, (ii) CuO nanoparticles, (iii) Cu (II) ions, (iv)

Elesclomol and Cu (II) ions, and (v) Elesclomol and CuO nanoparticles (Figure 5A–C). Elesclomol alone showed a negligible impact on viability of A549 cells, wherein 90% of the cells were viable at 50 ng/mL Elesclomol after 24 h (Figure 5A). The positive control (2% $\rm H_2O_2$) showed >95% reduction in the cell viability after 24 h exposure. The cell viability decreased to ~30 and ~40% at 100 and 1000 ng/mL Elesclomol exposure, respectively. Figure 5A shows that the exposure of lower concentrations of CuO nanoparticles (10–500 ng/mL) leads to >80% of A549 cell viability. However, the

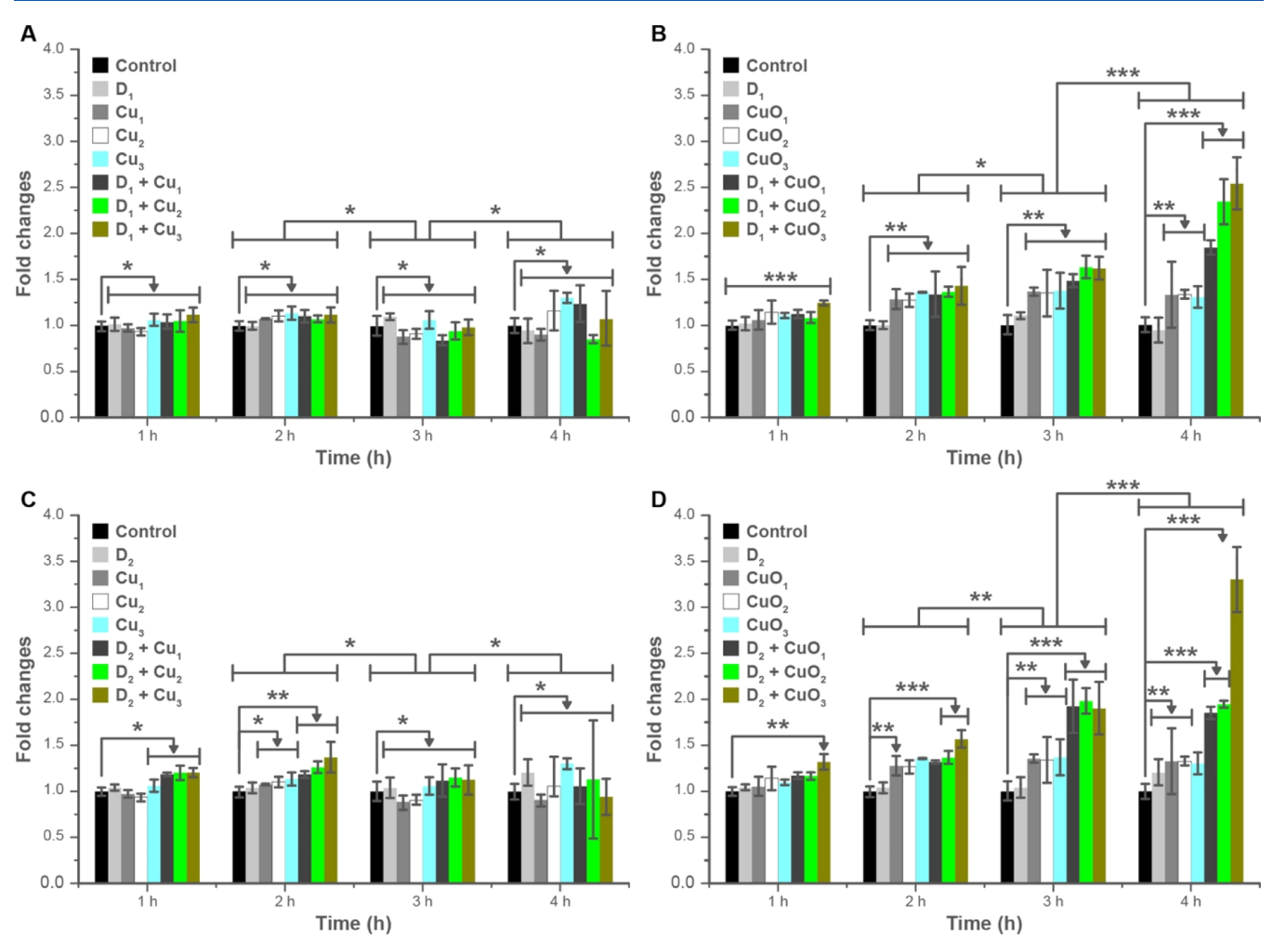


Figure 6. ROS generation on A549 cells exposed to different concentrations of Cu ions, CuO nanoparticles, drugs followed by DCFDA exposure for 30 min. (A) ROS generation on exposure to Cu ions and Elesclomol (10 ng/mL) combinations. (B) ROS generation on exposure to CuO nanoparticles and Elesclomol (10 ng/mL) combinations. (C) ROS generation on exposure to Cu ions and Elesclomol (50 ng/mL) combinations. (D) ROS generation on exposure to CuO nanoparticles and Elesclomol (50 ng/mL) combinations. The ROS generation was measured using a fluorescence spectrophotometer, and data represented in fold change compared with control. Data represented as mean \pm standard deviation (n = 3). *p < 0.05, **p < 0.01, and ***p < 0.001. Nomenclature—D₁: 10 ng/mL Elesclomol, D₂: 50 ng/mL Elesclomol, Cu₁: 50 ng/mL, Cu₂: 100 ng/mL, Cu₃: 200 ng/mL, CuO₁: 50 ng/mL, CuO₂: 100 ng/mL, and CuO₃: 200 ng/mL.

cell viability was found to be reduced to 22 and 40% at 1000 ng/mL and 10μ g/mL CuO nanoparticle exposure (Figure S8). In the case of Cu ions, the cell viability was reduced by 15 and 35% when exposed to 1 and 20 μ g/mL Cu ions, respectively (Figure S8). In cancer nanomedicine, the dosage or exposure concentration of nanoparticles is a critical component. The CuO nanoparticles are toxic to mammalian cells at a higher exposure concentration. Ahamed et al. (2010) reported that the standalone CuO nanoparticles are toxic to A549 cells in a dose-dependent manner by induction of lipid peroxidation, glutathione depletion, induction of superoxide dismutase, and so on. The cytotoxicity assay showed that at the exposure concentration of 10, 25, and 50 μ g/mL of CuO nanoparticles, the reduction in cell viability was observed to be 25, 34, and 52%, respectively.²⁸ However, at lower concentration, that is, <10 μ g/mL, the CuO nanoparticles are not significantly toxic to the mammalian cells and are in agreement with the cytotoxicity data reported in Figure S8. The exposure concentration of CuO nanoparticles used in our study was <0.5 μ g/mL, and at such a low exposure concentration, it is unlikely to have any harmful impact on the mammalian cells.

In a separate experiment, the Eleschomol drug (10-500 ng/ mL) was exposed to A549 cells in the presence of Cu ions (1 to 5000 ng/mL) (Figure 5B). After 24 h of incubation, there was a significant (***p < 0.001) decrease in cell viability after the exposure of increased Cu (II) ion concentration. We selected the Eleschomol concentration of 50 ng/mL for all our further experiments because (i) Elesclomol has a high affinity to bind with Cu (II) ions even at lower concentrations, (ii) of significant reduction in the cellular viability at 50 ng/mL Elesclomol concentration, and (iii) of reduction in the Elesclomol quantity and hence making it cost effective. Figure 5C shows a comparison of A549 cell viability on exposure to Cu ions, CuO nanoparticles, Elesclomol + Cu ions, and Elesclomol + CuO nanoparticles. After 24 h of exposure of CuO nanoparticles and Elesclomol, an exposure of 50 ng/mL nanoparticles and 50 ng/mL Elesclomol was enough to reduce the viability of A549 cells by 50%. Similarly, at a high exposure concentration of 250 and 500 ng/mL CuO nanoparticles, almost 90% of the cells were found to be dead. Interestingly, when CuO nanoparticles and 50 ng/mL Elesclomol were exposed together to A549 cells, there was a significant (***p <

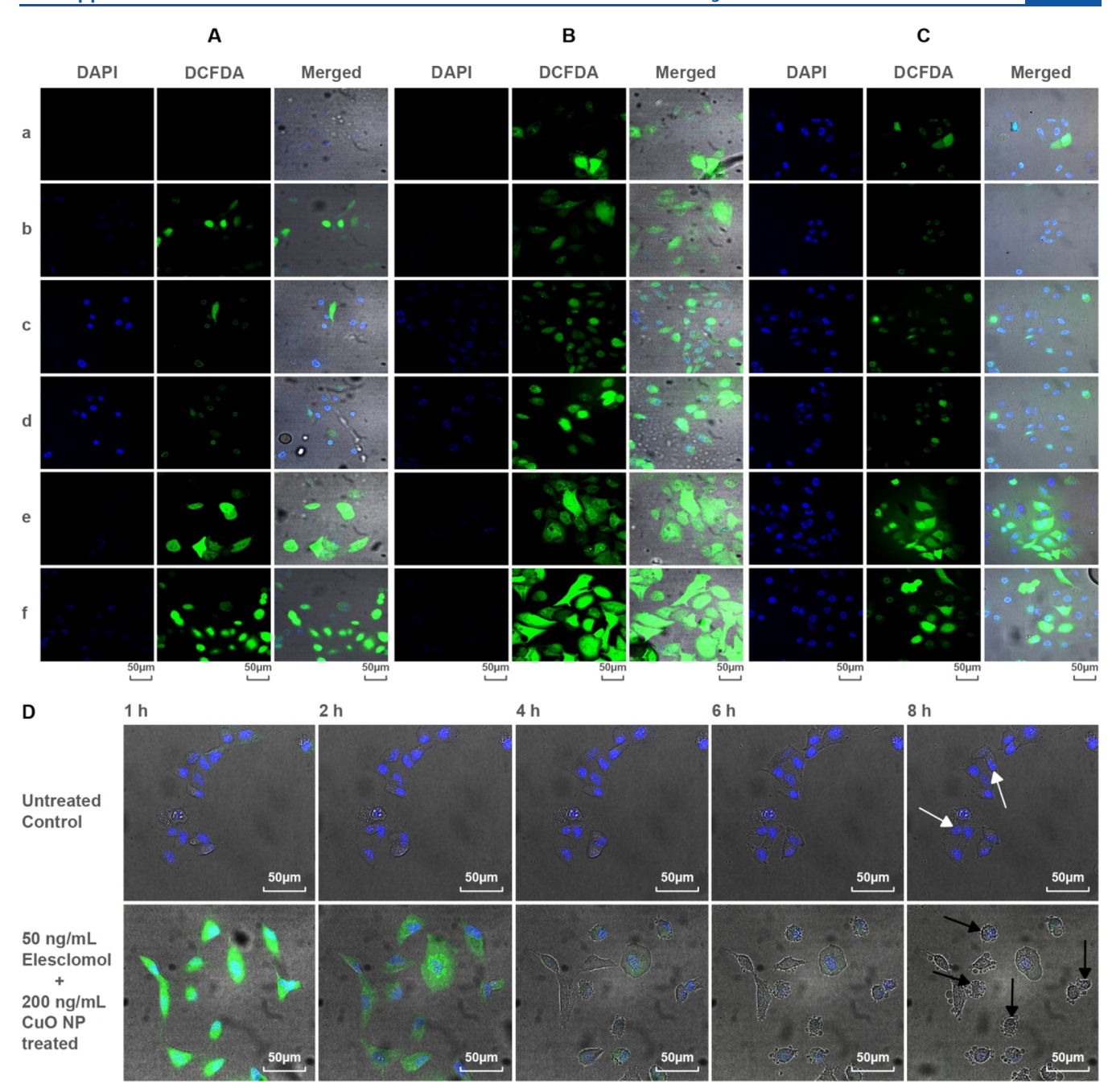


Figure 7. Pictomicrograph showing the time-dependent ROS production by A549 cells at 50 ng/mL Elesclomol and two different concentrations of CuO nanoparticles (100 and 200 ng/mL) (A) time = 1 h, (B) time = 2 h, and (C) time = 3 h (blue dye represents DAPI, and green dye represents DCFDA). (D) Live cell imaging snapshots collected from live cell video (SI video files) showing the A549 cells undergoing apoptosis after the end of 8 h of exposure to Elesclomol (50 ng/mL) + CuO nanoparticles (200 ng/mL) (blue dye represents Hoechst, and green dye represents DCFDA). Black arrow indicators represent A549 cells undergone apoptosis, and white arrow indicators represents healthy A549 cells. Legend nomenclature—a: Control, b: 50 ng/mL Elesclomol, c: 100 ng/mL CuO nanoparticles, d: 200 ng/mL CuO nanoparticles, e: 50 ng/mL Elesclomol + 100 ng/mL CuO nanoparticles, and f: 50 ng/mL Elesclomol + 200 ng/mL CuO nanoparticles.

0.001) reduction in the cell viability compared to all other combinations, for example, $85 \pm 4\%$ of cell viability when exposed to 50 ng/mL Elesclomol, $83 \pm 5\%$ viability when exposed to 50 ng/mL CuO nanoparticles, and $52 \pm 8\%$ viability when exposed to 50 ng/mL Elesclomol and 50 ng/mL CuO nanoparticles. Figure 5D represents a time-dependent (up to 24 h) A549 cell toxicity profile of A549 cells when exposed to (a) 50 ng/mL Elesclomol, (b) 500 ng/mL CuO nanoparticles, and (c) co-delivery of 500 ng/mL CuO nanoparticles and 50 ng/mL Elesclomol. Only Elesclomol

did not have any significant toxicity to the A549 cells (Figure 5D). For CuO nanoparticles, the cell viability was $78 \pm 3\%$ at the end of 24 h. However, in case of co-delivery of CuO nanoparticles with Elesclomol, the cell viability was reduced to $8.5 \pm 2\%$ after 24 h. In case of CuO nanoparticles and Elesclomol co-delivery, the cell viability reduced rapidly within 1 h of exposure, that is, $86 \pm 2\%$ in 0.25 h, $74 \pm 3\%$ in 0.5 h, and $71 \pm 4\%$ in 1 h. Microscopic imaging performed at 6 h showed the A549 cells to become spherical-shaped, which could be due to the loss of cell membrane integrity and

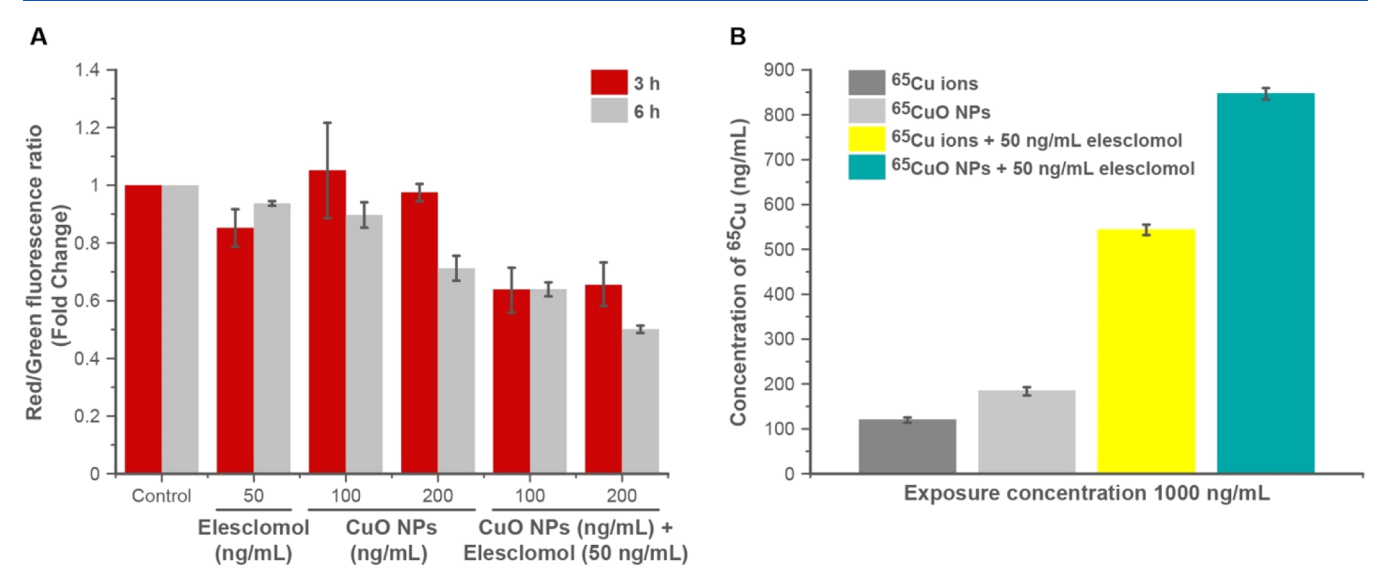


Figure 8. (A) Mitochondrial membrane potential assay showing decreased fold change in the red-to-green fluorescence ratio on exposure to CuO nanoparticles + Elesclomol. (B) Accumulation of 65 Cu in A549 cells on exposure to 1000 ng/mL 65 Cu ions and 65 CuO nanoparticles with or without 50 ng/mL Elesclomol for 3 h. Data represented as mean \pm standard deviation (n = 3).

approaching to apoptosis (Figures 5E and S4). At 8 and 12 h, majority of the cells underwent apoptosis, which is also in accordance with the time-dependent cytotoxic profile of A549 cells. Microscopic analysis showed that co-delivery of Elesclomol and CuO nanoparticles for 4 h could induce a significant impact on the cell morphology compared to the exposure of Elesclomol and CuO nanoparticles individually (Figure S5). On increasing the Elesclomol concentration from 10–100 ng/mL, more cells were found approaching apoptosis.

3.5. Co-delivery of Elesclomol and CuO Nanoparticles: Enhanced Oxidative Stress. Results from Figure 5D demonstrates that the cell viability starts reducing rapidly after the end of 3 h of CuO nanoparticles and Elesclomol exposure. Therefore, ROS production in A549 cells on exposure to 10 ng/mL Elesclomol with three different concentration of copper ions and CuO nanoparticles (50, 100, and 200 ng/mL) was followed from 1 to 4 h (Figure 6A,B). The reason of selecting 10 ng/mL Elesclomol was to demonstrate whether the drug is still efficient to generate ROS at concentration lesser than 50 ng/mL. The fold change in ROS generation was not significant when the cells were exposed to copper ions or Eleschomol, alone. For a combination of 10 ng/mL Elesclomol and 200 ng/mL Cu ions, exposed for 4 h, there was a 1.1-fold increase in ROS production. In contrast, there was a significant increase in ROS, such as 1.83-fold (10 ng/mL Elesclomol + 50 ng/mL CuO nanoparticles), 2.3-fold (10 ng/mL Elesclomol + 100 ng/ mL CuO nanoparticles), and 2.5-fold (10 ng/mL Elesclomol+ 200 ng/mL CuO nanoparticles). ROS production did not necessarily increase by increasing the Cu (II) concentration or the Elesclomol concentration. However, in case of Elesclomol + CuO nanoparticles exposure, there was a ~180% increase for 50 ng/mL Elesclomol + 50 ng/mL CuO nanoparticles, ~190% increase for 50 ng/mL Elesclomol + 100 ng/mL CuO nanoparticles, and ~330% increase for 50 ng/mL Elesclomol + 200 ng/mL CuO nanoparticles.

Figure 7A–C shows the confocal laser scanning microscopy (CLSM) images representing the time-dependent ROS production by A549 cells. At 1 h, the untreated control cell showed a minimal ROS production and some dead cells. As

compared to standalone treatment of CuO (100 ng/mL) nanoparticles and Elesclomol (50 ng/mL), very high ROS production was recorded when Elesclomol and CuO nanoparticles were co-delivered at equivalent concentrations. Similarly, the ROS production significantly increased after 2 h of exposure as compared to the control cells. 50 ng/mL Elesclomol co-delivered with 100 and 200 ng/mL CuO nanoparticles showed a very high ROS production after the exposure time of 2 h (Figure 7B). However, the fluorescent intensity of DCFDA dye was reduced significantly after the end of 3 h, and there was an increase in blue emission, suggesting the uptake of DAPI by dead cells (Figures 7C and S6). To appropriately quantify or image ROS production, the cells are required to be attached to the surface of the plate, and therefore, all our ROS quantifications were performed for the first 4 h. However, co-delivery of 10 ng/mL Elesclomol drug + CuO nanoparticles was not showing a significant impact on the cell morphology (Figure S4), ROS measurements (Figure 6B) demonstrated 10 ng/mL Elesclomol exposure to have substantial ROS generation after the end of 4 h.

Live cell imaging experiments were also performed to validate the intracellular ROS-mediated cellular death. For untreated cells used as control, the cells were healthy until the end of the experiment (12 h) with no significant abnormality observed. In case of standalone exposure of Elesclomol (50 ng/ mL) and CuO nanoparticles (200 ng/mL), majority of the cells were healthy, but there were few cell deaths observed after the end of 8 h. However, the co-delivery of Eleschomol (50 ng/ mL) and CuO nanoparticles (200 ng/mL) demonstrated a high ROS generation, which can be observed through the development of green fluorescence from the cells. The initial ROS generation (up to 3 h) goes in agreement with the ROS assay findings from flow cytometry and fluorescent spectroscopy analysis. It was also observed that most of the cells are undergoing apoptosis after the end of 8 h of the experiment. The live cell videos are attached in the Supplementary information file (Supplementary video files control.mp4, Elesclomol + CuO.mp4, only CuO treated.mp4, only Elesclomol treated.mp4). A time-dependent production of ROS and changes in the cell morphology in live cell imaging

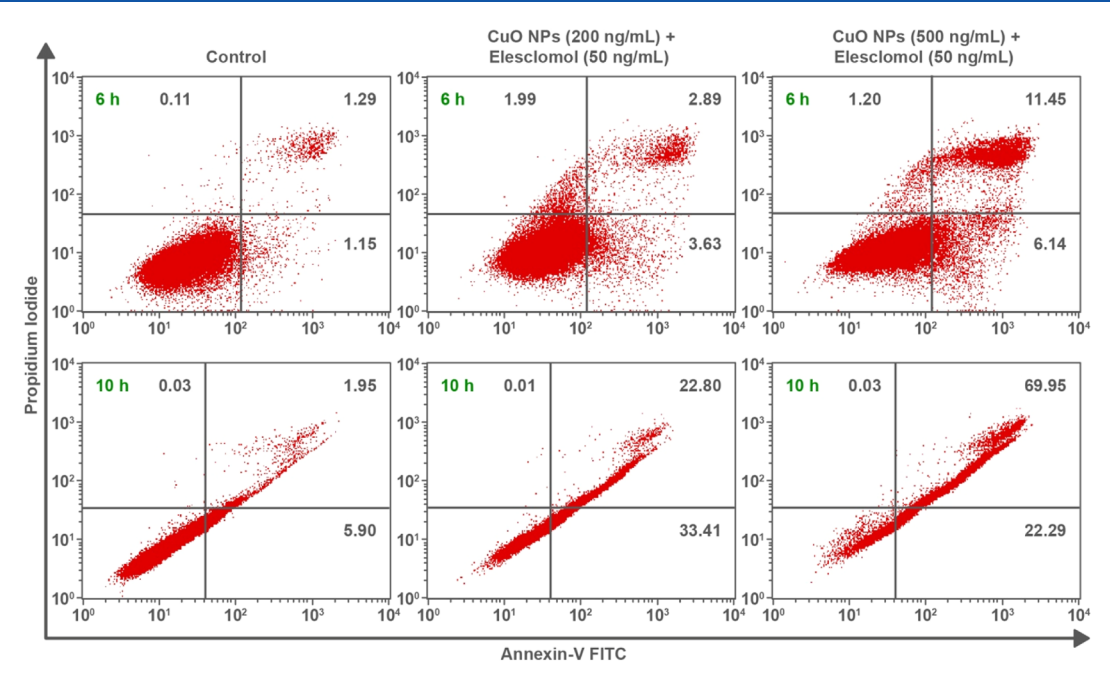


Figure 9. Time-dependent apoptosis/necrosis in AS49 cells exposed to Elesclomol, CuO nanoparticles, and CuO nanoparticles co-delivered with Elesclomol. Dot plot analysis of apoptotic cells by the annexin-V/PI staining after 6 h and 10 h treatment. Data represented as mean \pm standard error calculated from two individual experiments (n = 2).

have been shown in Figures 7D and Figure S7. In Figure 7D, the 8th h image marked with black arrow shows that the cells are undergoing apoptosis in case of co-delivery of Eleschomol (50 $\,$ ng/mL) and CuO nanoparticles (200 $\,$ ng/mL) due to enhanced ROS production, as demonstrated in initial time points.

3.6. Mitochondrial Membrane Depolarization. Loss in mitochondrial membrane potential is a key indicator for apoptosis and can be utilized to discriminate between healthy and apoptotic cells. We estimated the fold change in the redto-green fluorescence ratio with respect to control untreated cells. The red:green fluorescence ratio of JC-1 dye decreases with elevation in mitochondrial depolarization. As evident, from Figure 8A that Elesclomol and 100 ng/mL CuO nanoparticles show negligible changes in the red-to-green fluorescence ratio as compared to control, suggesting that it did not remarkably alter mitochondrial function. However, the increasing concentration of CuO nanoparticles (200 ng/mL) displayed a gradient decrease in red-to-green fluorescence ratio after 6 h treatment and was less than ~0.7 fold, suggesting mitochondrial depolarization. Interestingly, Elesclomol codelivered with CuO nanoparticles (100 ng/mL) caused ~0.65-fold change in the red-to-green fluorescence ratio after 3 and 6 h treatments. Furthermore, 6 h treatment of Elesclomol co-delivered with 200 ng/mL CuO nanoparticles showed more pronounce effect causing ~0.5-fold decrease in red-to-green fluorescence. Overall, the results suggested that 6 h exposure of Elesclomol co-delivered with CuO nanoparticles enhances the depolarization of mitochondrial membrane potential. The mitochondrial membrane depolarization initiates a cascade of events leading to the cellular apoptosis.

3.7. Elesclomol Facilitating High Intracellular Cu Trafficking. To establish that CuO nanoparticles acts as a reservoir for the slow and sustained release of copper ions to be ferried into the cell to be true, we quantified the intracellular total copper for A549 cells after exposure to stable isotopeenriched ⁶⁵CuO nanoparticles and Elesclomol treatment. The

stable isotope-labeled nanoparticles tracing takes place against the natural background and majorly reliant on measuring the isotopic changes in the biological cells that result from the exposure of nanoparticles synthesized using enriched isotopic constituent. 100% ⁶⁵Cu-enriched ⁶⁵CuO nanoparticles were synthesized, with similar physicochemical properties to nonisotopically labeled CuO nanoparticles. The background concentration of 65 Cu was measured to be 19.37 \pm 3.2 ng/ mL in A549 cells. The A549 cells were exposed with 1000 ng/ mL ⁶⁵Cu ions and 1000 ng/mL ⁶⁵CuO nanoparticles with and without 50 ng/mL Elesclomol. After 3 h of incubation without Elesclomol (Figure 8B), the total cellular concentration of 65 Cu was found to be 120.5 \pm 4.8 ng/mL when the ionic tracer was used (i.e., ⁶⁵Cu ions), whereas for ⁶⁵CuO nanoparticles, the accumulation of 65Cu inside the cells was measured as 184.05 ± 7.6 ng/mL. The reason of increase in the cellular concentration of ⁶⁵Cu ions from ⁶⁵CuO nanoparticles exposure can be because of internalization and accumulation of 65CuO nanoparticles itself into the cells. In the presence of 50 ng/mL Elesclomol, the concentration of 65Cu increased in the cells increased significantly for both 65Cu ions and 65CuO nanoparticles. The measured concentration of ⁶⁵Cu was 544 \pm 10.4 and 847 \pm 11 ng/mL for ⁶⁵Cu ionic exposure and ⁶⁵CuO nanoparticulate exposure. According to the dissolution profile of CuO in DMEM (10% FBS) media, 71.4 ± 2 wt % of CuO gets dissolved within 3 h of its exposure to media. It signifies that more extracellular copper ions were available to Elesclomol molecules from dissolution of 65CuO nanoparticles to transport inside the cells as compared to the standalone exposure of 65Cu ions. On investigating the amount of 65Cu ions remaining in the media, it was found that $390 \pm 4 \text{ ng/mL}$ from only 65 Cu ion samples and 133.4 \pm 6 ng/mL from 65 CuO samples were still present in the samples either in the form of ⁶⁵Cu complexes or undissolved ⁶⁵CuO nanoparticles.

3.8. Cancer Cells Undergoing Apoptosis on Exposure to CuO and Elesclomol. An important hallmark for

apoptosis is externalization of phosphatidylserine to the outer leaflet of the cell membrane, which can be experimentally quantified by the annexin V binding. Annexin V/PI double positive cells signify the apoptotic cell population. Likewise, 6 h exposure of Elesclomol (50 ng/mL) co-delivered with CuO nanoparticles (500 ng/mL) demonstrated the increase in the apoptotic cell population by \sim 11.45% with most of the cells in late apoptotic stage (Annexin-V/PI double positive, Figure 9). However, 10 h treatment showed a drastic increase in apoptotic cell population by ~22.80% for Elesclomol (50 ng/mL) co-delivered with CuO nanoparticles (200 ng/mL) and by ~69.90% Elesclomol (50 ng/mL) co-delivered with CuO nanoparticles (500 ng/mL). The data are in agreement with the live cell imaging (Figure 7D) and cytotoxicity assays (Figure 5) that show there was an enhanced ROS production until 3-4 h of the CuO and Elesclomol exposure, and later, the cells are undergoing apoptosis after 6-8 h.

3.9. Proposed Mechanism for Enhanced Oxidative Stress Generation. The Eleschomol drug is known to preferentially bind with copper ions and acts as a shuttle to transport Cu ions inside the cells and more specifically to mitochondria. The proposed mechanism of enhanced ROS generation is shown in Figure 1. Briefly, once inside the cell, the major cause of cellular toxicity of Cu (II) ions is due to the generation of ROS. The shuttling of Cu (II) ions by Elesclomol is a spontaneous process wherein once the Cu (II) ions are delivered inside the mitochondria by the drug molecule; due to a reducing environment in mitochondria, the Cu (II) in the Cu (II)–Elesclomol complex gains one electron and reduces to Cu (I). Once the reduction happens, the Cu (I) gets out of the complex and creates an alteration in the electron transport chain and generates ROS by the Fenton-like reaction. The free Elesclomol gets effluxes out of the cells to complex with other free Cu (II) ions present outside the cell and repeat the entire shuttling process.⁵ The presence of Cu (I) ions becomes the source of generation of hydroxyl radicals (OH·) due to the Fenton reaction.²⁶ As shown in Figure 1, cuprous ions react with mitochondrial hydrogen peroxide and build up high concentration of hydroxyl radicals inside the cells. The excess buildup of ROS (OH·) inside the cells can induce damages to lipids, proteins, nucleic acids, and organelles and further lead to apoptosis through the activation of caspase pathways.²

Therefore, the observations from Figure 5B suggest that it is important that free Cu (II) ions must be available at extracellular milieu so that the drug can make an active complex with Cu (II) ions. However, in a complex cell culture media such as DMEM, there are various other Cu complexforming agents such as ascorbate, glutamic acid, folic acid, and so on that can quickly form complex with Cu (II) and reduce the number of free available Cu (II) ions to form complex with Elesclomol causing lower amount of Cu (II) ions to be transported inside the cells and generate oxidative stress. The MD- and DFT-based studies suggested that even in the presence of Cu-complex forming agents like amino acids, dissolved Cu (II) ions generated from dissolution of CuO nanoparticles preferentially bind to Elesclomol. This will help in increased Elesclomol-mediated transportation of Cu (II) through redox chemistry and induce lethal oxidative stress. This enhanced toxicity toward A549 cells could be explained by the dissolution profile of CuO nanoparticles (Figure 3A). 85.2 ± 3.6 wt % of CuO nanoparticles dissolves after 24 h. It also demonstrated that significant amount of dissolved Cu (II)

ions are already available for Elesclomol to be transported inside the mitochondria and generate enhanced oxidative stress. The CuO nanoparticles act as a reservoir from which a gradual release of copper ions happens, thus allowing Elesclomol to bind and shuttle Cu (II) inside the cell. In comparison, Cu (II) ions easily form complexes as soon as it is exposed to cell culture media, which reduces the Cu (II)-Elesclomol complexation and its intracellular trafficking. Due to the shuttling mechanism of the Eleschomol, the free Cu (II) ions availability becomes the limiting factor because the majority of Cu (II) ions form complexes with various complexforming agents. However, in case of CuO nanoparticles, the slow and sustained release of Cu ions allows a time lag for free Elesclomol molecules to complex with available free Cu (II) and transports it inside the mitochondria. The dissolution of CuO nanoparticles, therefore, provides a constant supply of Cu (II) ions for a longer duration to Eleschomol and hence makes it a better candidate for inducing prolonged oxidative stress. According to Du et al. (2020), 25 there is a positive correlation between the ROS production with that of dissociation constant (pK_a) of an organic compound. The reported theoretically calculated pK_a value of 11.41 for the Eleschomol-Cu(II) complex is considered to be higher in the reducing environment like mitochondria. We expect a significant difference in the antitumor activity in vivo because of various other underlying reasons [e.g., enhanced permeation and retention (EPR) effect and rapid angiogenesis. The parameters like the EPR effect and rapid angiogenesis are not present in normal cells. However, the tumor cells have elevated ROS levels as compared to normal cells, the enhanced oxidative stress increases the ROS level and exhausts the antioxidant capacity of the tumor, resulting in apoptotic pathways. The cancer cells operate with higher ROS level with reduced anti-oxidant capacity than normal cells. These unique features make cancer cells more vulnerable to Elesclomol-Cu (II) complexes that enhance the oxidative stress.

4. CONCLUSIONS

In our study, CuO nanoparticles were found to act as a reservoir of copper ions, facilitating slow and controlled dissolution in the cell culture media offering a sustained and steady supply of copper ions for Elesclomol to bind. Cytotoxicity and ROS experiments demonstrated that the percentage of cell death and ROS generation were very high during the initial time and was sustained after that. The generated dissolved species allowed the Elesclomol molecules to shuttle these dissolved Cu ions inside the mitochondria to produce ROS-mediated cell death. The activity of the Cu-Elesclomol complex was rapid, with approximately 80% of the cell death occurring within 12 h. The dissolved ions from CuO nanoparticles readily formed a complex with the Elesclomol drug and were transported to mitochondria to generate intracellular ROS. The theoretical values provide support to the correct assignment of a 360 nm plateau region observed in the experimental spectra, due to the formation of the Cu (II)-Elesclomol complex. 50 ng/mL Elesclomol when codelivered with 50-100 ng/mL of CuO nanoparticles was enough to reduce the cell viability by >50%. As demonstrated through ROS quantification and live cell imaging, the ROS production in A549 cells are at its peak at 3-4 h after the exposure of 50 ng/mL Elesclomol and 100 ng/mL CuO nanoparticles. Through live cell imaging and ROS quantification, it was observed that the cells were generating high ROS

up to 3–4 h, loss of membrane integrity at 4–6 h, and undergoing apoptosis after 6 h. The stable isotope labeling approach helped demonstrating a high amount of Cu ions being trafficked inside the cells. It also demonstrated that only extracellular Cu ions being trafficked inside the cells through the shuttling mechanism of Eleschomol drug. The co-delivery approach minimized the Eleschomol dosage requirement (50 ng/mL) compared to some of the other anticancer drugs commonly used as anticancer agents. The nanoparticle enabled co-delivery route showed a promising approach toward the toxicity of cancer cells through CuO nanoparticle dissolution-mediated oxidative stress-based anticancer therapy.

ASSOCIATED CONTENT

3 Supporting Information

The Supporting Information is available free of charge at https://pubs.acs.org/doi/10.1021/acsanm.1c04350.

Data from the published literature on the efficacy of Elesclomol; characterization of ⁶⁵CuO nanoparticles; time-dependent stability of Elesclomol in DMEM; DFT methodology and data set; and cell morphology and ROS imaging data set (PDF)

Control (MP4)

Elesclomol + CuO (MP4)

Only CuO treated (MP4)

Only Elesclomol-treated file for live cell imaging of ROS production (MP4)

AUTHOR INFORMATION

Corresponding Authors

Swaroop Chakraborty – Materials Engineering, Indian Institute of Technology Gandhinagar, Gandhinagar 382355, India; School of Geography, Earth & Environmental Sciences, University of Birmingham, Birmingham B152TT, U.K.; orcid.org/0000-0002-4388-4964;

Email: s.chakraborty@bham.ac.uk

Superb K. Misra – Materials Engineering, Indian Institute of Technology Gandhinagar, Gandhinagar 382355, India;

orcid.org/0000-0001-5551-2706; **Email:** smisra@ iitgn.ac.in

Authors

Prabhat Prakash — Materials Engineering, Indian Institute of Technology Gandhinagar, Gandhinagar 382355, India; orcid.org/0000-0003-1430-2379

Juhi Shah – Division of Biological and Life Sciences, Ahmedabad University, Ahmedabad 380009, India

Chaithra Mayya — Biological Engineering, Indian Institute of Technology Gandhinagar, Gandhinagar 382355, India

Sanjay Singh – Division of Biological and Life Sciences, Ahmedabad University, Ahmedabad 380009, India; orcid.org/0000-0002-6256-7091

Raghavan Ranganathan — Materials Engineering, Indian Institute of Technology Gandhinagar, Gandhinagar 382355, India; © orcid.org/0000-0003-1015-791X

Virupakshi Soppina — Biological Engineering, Indian Institute of Technology Gandhinagar, Gandhinagar 382355, India; orcid.org/0000-0003-1196-7770

Eugenia Valsami Jones — School of Geography, Earth & Environmental Sciences, University of Birmingham, Birmingham B152TT, U.K.; orcid.org/0000-0002-8850-7556

Complete contact information is available at: https://pubs.acs.org/10.1021/acsanm.1c04350

Author Contributions

S.C.: Conceptualization, methodology, validation, investigation, formal analysis, writing, visualization, and editing. P.P.: Investigation, formal analysis, and writing, J.S.: Investigation, formal analysis, writing. C.M.: Investigation. R.R.: Conceptualization. V.S.: Conceptualization and editing. S.S.: Visualization and editing. E.V.J.: Visualization and editing. S.K.M.: Conceptualization, visualization, and editing.

Funding

This work has been financially supported by the IMPRINT (project no. 6408, MHRD) and SERB-CRG (CRG/2019/006165). V.S. acknowledges funding through DBT (grant nos. BT/PR15214/BRB/10/1449/2015 and BT/RLF/re-entry/45/2015) and DST-SERB (grant no. ECR/2016/000913).

Notes

The authors declare no competing financial interest.

ACKNOWLEDGMENTS

We acknowledge Dr. Dhiraj Bhatia's (Assistant Professor, IIT Gandhinagar) support with live cell imaging of the samples. We also acknowledge Chantal Jackson (University of Birmingham, UK) to support us with formatting the figures used in the manuscript.

REFERENCES

- (1) Angelé-Martínez, C.; Nguyen, K. V. T.; Ameer, F. S.; Anker, J. N.; Brumaghim, J. L. Reactive Oxygen Species Generation by Copper(II) Oxide Nanoparticles Determined by DNA Damage Assays and EPR Spectroscopy. *Nanotoxicology* **2017**, *11*, 278.
- (2) Vinardell, M.; Mitjans, M. Antitumor Activities of Metal Oxide Nanoparticles. *Nanomaterials* **2015**, *5*, 1004.
- (3) Postovit, L.; Widmann, C.; Huang, P.; Gibson, S. B. Harnessing Oxidative Stress as an Innovative Target for Cancer Therapy. *Oxid. Med. Cell. Longevity* **2018**, 2018, 6135739.
- (4) Kirshner, J. R.; He, S.; Balasubramanyam, V.; Kepros, J.; Yang, C.-Y.; Zhang, M.; Du, Z.; Barsoum, J.; Bertin, J. Elesclomol Induces Cancer Cell Apoptosis through Oxidative Stress. *Mol. Cancer Ther.* **2008**, *7*, 2319–2327.
- (5) Nagai, M.; Vo, N. H.; Shin Ogawa, L.; Chimmanamada, D.; Inoue, T.; Chu, J.; Beaudette-Zlatanova, B. C.; Lu, R.; Blackman, R. K.; Barsoum, J.; Koya, K.; Wada, Y. The Oncology Drug Elesclomol Selectively Transports Copper to the Mitochondria to Induce Oxidative Stress in Cancer Cells. *Free Radical Biol. Med.* **2012**, *52*, 2142–2150.
- (6) Yadav, A. A.; Patel, D.; Wu, X.; Hasinoff, B. B. Molecular Mechanisms of the Biological Activity of the Anticancer Drug Elesclomol and Its Complexes with Cu(II), Ni(II) and Pt(II). *J. Inorg. Biochem.* **2013**, 126, 1–6.
- (7) Carloni, P.; Rothlisberger, U.; Parrinello, M. The Role and Perspective of Ab Initio Molecular Dynamics in the Study of Biological Systems. *Acc. Chem. Res.* **2002**, *35*, 455–464.
- (8) De Vivo, M.; Masetti, M.; Bottegoni, G.; Cavalli, A. Role of Molecular Dynamics and Related Methods in Drug Discovery. *J. Med. Chem.* **2016**, *59*, 4035–4061.
- (9) Tidjani-Rahmouni, N.; Bensiradj, N. E. H.; Djebbar, S.; Benali-Baitich, O. Synthesis, Characterization, Electrochemical Studies and DFT Calculations of Amino Acids Ternary Complexes of Copper (II) with Isonitrosoacetophenone. Biological Activities. *J. Mol. Struct.* **2014**, *1075*, 254–263.
- (10) Wu, Z.; Fernandez-Lima, F. A.; Russell, D. H. Amino Acid Influence on Copper Binding to Peptides: Cysteine versus Arginine. *J. Am. Soc. Mass Spectrom.* **2010**, *21*, 522–533.

- (11) Utembe, W.; Potgieter, K.; Stefaniak, A. B.; Gulumian, M. Dissolution and Biodurability: Important Parameters Needed for Risk Assessment of Nanomaterials. *Part. Fibre Toxicol.* **2015**, *12*, 11.
- (12) Chakraborty, S.; Nair, A.; Paliwal, M.; Dybowska, A.; Misra, S. K. Exposure Media a Critical Factor for Controlling Dissolution of CuO Nanoparticles. *J. Nanopart. Res.* **2018**, *20*, 331.
- (13) Jorgensen, W. L.; Maxwell, D. S.; Tirado-Rives, J. Development and Testing of the OPLS All-Atom Force Field on Conformational Energetics and Properties of Organic Liquids. *J. Am. Chem. Soc.* **1996**, 118, 11225–11236.
- (14) Wu, L.; Zhou, L.; Liu, D. Q.; Vogt, F. G.; Kord, A. S. LC-MS/MS and Density Functional Theory Study of Copper(II) and Nickel(II) Chelating Complexes of Elesclomol (a Novel Anticancer Agent). *J. Pharm. Biomed. Anal.* **2011**, *54*, 331.
- (15) Spackman, M. A. Potential Derived Charges Using a Geodesic Point Selection Scheme. *J. Comput. Chem.* **1996**, *17*, 1–18.
- (16) Shah, M. R.; Imran, M.; Ullah, S. Nanocarrier-Based Targeted Pulmonary Delivery: Novel Approaches for Effective Lung Cancer Treatment. *Nanocarriers for Cancer Diagnosis and Targeted Chemotherapy*; Elsevier, 2019; pp 129–161.
- (17) Abraham, M. J.; Murtola, T.; Schulz, R.; Páll, S.; Smith, J. C.; Hess, B.; Lindahl, E. Gromacs: High Performance Molecular Simulations through Multi-Level Parallelism from Laptops to Supercomputers. *SoftwareX* **2015**, *1*–2, 19–25.
- (18) Frisch, M. J.; Trucks, G. W.; Schlegel, H. B.; Scuseria, G. E.; Robb, M. A.; Cheeseman, J. R.; Scalmani, G.; Barone, V.; Mennucci, B.; Petersson, G. A.; Nakatsuji, H.; Caricato, M.; Li, X.; Hratchian, H. P.; Izmaylov, A. F.; Bloino, J.; Zheng, G.; Sonnenberg, J. L.; Hada, M.; Ehara, M.; Toyota, K.; Fukuda, R.; Hasegawa, J.; Ishida, M.; Nakajima, T.; Honda, Y.; Kitao, O.; Nakai, H.; Vreven, T.; Montgomery, Jr., J. A.; Peralta, J. E.; Ogliaro, F.; Bearpark, M.; Heyd, J. J.; Brothers, E.; Kudin, K. N.; Staroverov, V. N.; Kobayashi, R.; Normand, J.; Raghavachari, K.; Rendell, A.; Burant, J. C.; Iyengar, S. S.; Tomasi, J.; Cossi, M.; Rega, N.; Millam, J. M.; Klene, M.; Knox, J. E.; Cross, J. B.; Bakken, V.; Adamo, C.; Jaramillo, J.; Gomperts, R.; Stratmann, R. E.; Yazyev, O.; Austin, A. J.; Cammi, R.; Pomelli, C.; Ochterski, J. W.; Martin, R. L.; Morokuma, K.; Zakrzewski, V. G.; Voth, G. A.; Salvador, P.; Dannenberg, J. J.; Dapprich, S.; Daniels, A. D.; Farkas, Ö.; Foresman, J. B.; Ortiz, J. V.; Cioslowski, J.; Fox, D. J. Gaussian O9 Revision D.01; Gaussian Inc.: Wallingford CT. Gaussian 09 Revision C.01, 2010.
- (19) Perdew, J. P.; Burke, K.; Ernzerhof, M. Generalized Gradient Approximation Made Simple. *Phys. Rev. Lett.* **1996**, *77*, 3865–3868.
- (20) Hay, P. J.; Wadt, W. R. Ab Initio Effective Core Potentials for Molecular Calculations. Potentials for the Transition Metal Atoms Sc to Hg. J. Chem. Phys. 1985, 82, 270–283.
- (21) Mosmann, T. Rapid Colorimetric Assay for Cellular Growth and Survival: Application to Proliferation and Cytotoxicity Assays. *J. Immunol. Methods* **1983**, *65*, 55–63.
- (22) Chakraborty, S.; Mahadevan, B. K.; Shah, J.; Panse, K.; Malvi, B.; Balasubramanian, C.; Singh, S.; Misra, S. K. Enhanced Detection Using Stable Isotope Enriched 65Cu Doped Ferrite Nanoparticles for Tracing Studies. *J. Alloys Compd.* 2020, 822, 153502.
- (23) Misra, S. K.; Dybowska, A.; Berhanu, D.; Luoma, S. N.; Valsami-Jones, E. The Complexity of Nanoparticle Dissolution and Its Importance in Nanotoxicological Studies. *Sci. Total Environ.* **2012**, 438, 225–232.
- (24) Chakraborty, S.; Misra, S. K. A Comparative Analysis of Dialysis Based Separation Methods for Assessing Copper Oxide Nanoparticle Solubility. *Environ. Nanotechnol. Monit. Manag.* **2019**, 12, 100258.
- (25) Du, Q.; Jia, W.; Dai, J.; Du, C.; Shao, A.; Zhang, R.; Ji, Y. Effect of Dissociation Constant (PKa) of Natural Organic Matter on Photo-Generation of Reactive Oxygen Species (ROS). *J. Photochem. Photobiol.*, A **2020**, 391, 112345.
- (26) Raha, S.; Robinson, B. H. Mitochondria, Oxygen Free Radicals, Disease and Ageing. *Trends Biochem. Sci.* **2000**, *25*, 502–508.

- (27) Redza-Dutordoir, M.; Averill-Bates, D. A. Activation of Apoptosis Signalling Pathways by Reactive Oxygen Species. *Biochim. Biophys. Acta, Mol. Cell Res.* **2016**, 1863, 2977–2992.
- (28) Ahamed, M.; Siddiqui, M. A.; Akhtar, M. J.; Ahmad, I.; Pant, A. B.; Alhadlaq, H. A. Genotoxic Potential of Copper Oxide Nanoparticles in Human Lung Epithelial Cells. *Biochem. Biophys. Res. Commun.* 2010, 396, 578–583.

Recommended by ACS

A Self-Assembled Copper-Selenocysteine Nanoparticle for Enhanced Chemodynamic Therapy via Oxidative Stress Amplification

Ziyi Chen, Xiankun Tu, et al.

MARCH 21, 2023

ACS MATERIALS LETTERS

READ 🗹

A Stepwise-Confined Self-Reduction Strategy to Construct a Dynamic Nanocatalyst for Boosting Tumor Catalytic Therapy

Qiqi Sun, Dechao Niu, et al.

DECEMBER 22, 2022

CHEMISTRY OF MATERIALS

READ 🗹

 $Heterostructural\ Nanoadjuvant\ CuSe/CoSe_2\ for\ Potentiating\ Ferroptosis\ and\ Photoimmunotherapy\ through\ Intratumoral\ Blocked\ Lactate\ Efflux$

Chunzheng Yang, Jun Lin, et al.

MARCH 23, 2023

JOURNAL OF THE AMERICAN CHEMICAL SOCIETY

READ 🗹

Coordination-Driven Self-Assembly Strategy-Activated Cu Single-Atom Nanozymes for Catalytic Tumor-Specific Therapy

Jie Zhou, Yuliang Zhao, et al.

FEBRUARY 06, 2023

JOURNAL OF THE AMERICAN CHEMICAL SOCIETY

READ 🗹